

Obesity and altered glucose metabolism impact HDL composition in CETP transgenic mice: a role for ovarian hormones[§]

Melissa N. Martinez,* Christopher H. Emfinger,^{†,§} Matthew Overton,^{*,***} Salisha Hill,^{††} Tara S. Ramaswamy,* David A. Cappel,* Ke Wu,^{§,§§} Sergio Fazio,^{***} W. Hayes McDonald,^{†††} David L. Hachey,^{†††} David L. Tabb,^{††} and John M. Stafford^{1,*,†,§}

Tennessee Valley Healthcare System,[†] Division of Diabetes, Endocrinology, & Metabolism,[§] Department of Molecular Physiology & Biophysics,* Department of Biomedical Informatics,^{††} Atherosclerosis Research Unit, Division of Cardiovascular Medicine,^{***} Mass Spectroscopy Research Center Vanderbilt University School of Medicine,^{†††} Wuhan University,^{§§} University of North Carolina, Chapel Hill^{**}

Abstract Mechanisms underlying changes in HDL composition caused by obesity are poorly defined, partly because mice lack expression of cholesteryl ester transfer protein (CETP), which shuttles triglyceride and cholesteryl ester between lipoproteins. Because menopause is associated with weight gain, altered glucose metabolism, and changes in HDL, we tested the effect of feeding a high-fat diet (HFD) and ovariectomy (OVX) on glucose metabolism and HDL composition in CETP transgenic mice. After OVX, female CETP-expressing mice had accelerated weight gain with HFD-feeding and impaired glucose tolerance by hyperglycemic clamp techniques, compared with OVX mice fed a low-fat diet (LFD). Sham-operated mice (SHAM) did not show HFD-induced weight gain and had less glucose intolerance than OVX mice. Using shotgun HDL proteomics, HFD-feeding in OVX mice had a large effect on HDL composition, including increased levels of apoA2, apoA4, apoC2, and apoC3, proteins involved in TG metabolism. These changes were associated with decreased hepatic expression of SR-B1, ABCA1, and LDL receptor, proteins involved in modulating the lipid content of HDL. In SHAM mice, there were minimal changes in HDL composition with HFD feeding. **¶** These studies suggest that the absence of ovarian hormones negatively influences the response to high-fat feeding in terms of glucose tolerance and HDL composition. CETP-expressing mice may represent a useful model to define how metabolic changes affect HDL composition and function.—Martinez, M. N., C. H. Emfinger, M. Overton, S. Hill, T. S.

Ramaswamy, D. A. Cappel, K. Wu, S. Fazio, W. H. McDonald, D. L. Hachey, D. L. Tabb, and J. M. Stafford. Obesity and altered glucose metabolism impact HDL composition in CETP transgenic mice: a role for ovarian hormones. *J. Lipid Res.* 2012. 53: 379–389.

Supplementary key words triglycerides • menopause • proteomics • hyperglycemic clamp • high density lipoprotein • cholesteryl ester transfer protein

Impairment in HDL function associated with obesity and elevated serum triglyceride (TG) may be a major contributor to risk of coronary heart disease (CHD) in obese patients, yet mechanisms by which changes in metabolism impair HDL function are not well defined (1–6). Increased TGs in the form of VLDL give rise to low levels of HDL in part due to the actions of cholesteryl ester transfer protein (CETP), which shuttles TG and cholesteryl esters between serum lipoproteins. Because of lipid exchange, elevated serum VLDL leads to TG enrichment of HDL. This TG enrichment reduces the affinity of apolipoprotein A1 (apoA1) for cholesterol, promotes clearance of apoA1, and decreases HDL particle number (1, 3, 7). In addition, changes in the function of HDL related to inflammation, coagulation, and reverse cholesterol transport are associated with obesity and metabolic diseases. HDL proteomics have revealed changes in apolipoproteins, inflammatory proteins, and coagulation proteins in individuals with known

This work was supported by the Department of Veterans Affairs, the American Heart Association (10GRNT3650024), Atlantic Philanthropies Inc., American Diabetes Association (1-09-IG-01), the John A. Hartford Foundation, and the Association of Specialty Professors, the Vanderbilt Diabetes Research and Training Center Pilot and Feasibility Program (NIHDK020593), the Vanderbilt Digestive Diseases Research Center Pilot and Feasibility Program (DK058404), a Vanderbilt Reproductive Biology Training Grant (M.M.), and a Vanderbilt Molecular Endocrinology Training Grant (D.C.). Proteome informatics was supported by R01 CA126218 and U01 CA152647 from the National Institutes of Health. The contents of this article are solely the responsibility of the authors and do not necessarily represent the official views of the National Institutes of Health or other granting agencies..

Manuscript received 26 August 2011 and in revised form 15 December 2011.

Published, *JLR Papers in Press*, January 3, 2012
DOI 10.1194/jlr.M019752

Copyright © 2012 by the American Society for Biochemistry and Molecular Biology, Inc.

This article is available online at <http://www.jlr.org>

Abbreviations: CETP, cholesteryl ester transfer protein; HFD, high-fat diet; LDLR, low-density lipoprotein receptor; LFD, low-fat diet; OVX, ovariectomy; SR-B1, scavenger receptor class B1; SREBP-1c, sterol regulatory binding protein 1c; TG, triglyceride.

¹To whom correspondence should be addressed.

e-mail: john.stafford@vanderbilt.edu

§ The online version of this article (available at <http://www.jlr.org>) contains supplementary data in the form of five tables.

CHD compared with control subjects (8–12). These functional properties of HDL are known to predict CHD risk independently of HDL cholesterol levels (4, 13–17). However, due to the chronic nature of cardiovascular disease in humans, it is unclear how acute changes in metabolism result in changes in HDL composition.

In women, menopause represents a transition in cardiovascular risk associated with obesity, abnormal glucose metabolism, and dyslipidemia characterized by increased VLDL-TG and decreased HDL (18–20). Despite strong associations of postmenopausal obesity and impaired glucose tolerance, the impact of these changes on HDL composition has been difficult to explore, partly because the most common model of metabolic disease, the mouse, lacks CETP expression. CETP transgenic mice display a lipid profile with elevated VLDL and LDL and decreased HDL and are an established model of atherosclerosis (21–23). The proteome of HDL in CETP mice, and its relationship to HDL composition in humans, is not known. We proposed that we could use CETP-expressing mice to define how metabolic changes associated with obesity affect HDL composition.

Our overall objective was to define how alterations in glucose and TG metabolism associated with obesity affect HDL composition. We used ovariectomy (OVX) as a model of menopause because after OVX mice are susceptible to diet-induced obesity and impairments in glucose and TG metabolism. Two strains of CETP-expressing mice have been commonly used to study the impact of CETP expression on lipid metabolism. In humans and in mice expressing the human CETP gene, CETP expression is induced with obesity, is suppressed by acute hyperinsulinemia, and is regulated by ovarian hormones (23–26). We used mice that constitutively express the simian CETP gene (22, 27) to define how metabolic changes affect HDL composition, independent of alterations in CETP expression. To define metabolic conditions that related to alterations in HDL composition, we performed hyperglycemic clamp techniques to define glucose tolerance. Glucose tolerance *in vivo* represents the integration of blood glucose changes and changes in serum insulin that result from glucose changes. The hyperglycemic clamp approach allowed us to provide a matched-change in blood glucose levels between groups and thus define the effect of HFD feeding and OVX on glucose tolerance and the insulin secretory response. We then performed shotgun proteomics of HDL to define changes in HDL proteins after HFD feeding and OVX. HFD feeding had a greater effect on glucose tolerance and HDL composition after OVX. These studies suggest a differential impact of obesity and HFD feeding on HDL protein composition after the loss of ovarian hormones.

METHODS

Animals

CETP transgenic mice on a C57BL6 genetic background (C57BL/6-Tg(CETP)1Pnu/J, stock number 001929) were purchased from The Jackson Laboratory (Bar Harbor, Maine). All

mice were maintained on a standard chow diet until placement on a LFD (10% fat from lard, 70% carbohydrate, 20% protein, Research Diets D01060501) or a HFD (60% fat from lard, 20% carbohydrate, 20% protein, Research Diets D08060104). The diets are micronutrient matched. The fat derives from lard (32% saturated fat, 36% monounsaturated fat, 32% polyunsaturated fat), and the carbohydrate from cornstarch. All procedures were performed in accordance with National Institutes of Health Guidelines for the Care and Use of Animals and were approved by the Institutional Animal Care and Use Committee at Vanderbilt University.

Surgical ovariectomy

Female mice (12 weeks old) were laid on their ventral surface with tail toward the surgeon. A small midline dorsal incision was made halfway between the base of the tail and mid-back. The peritoneal cavity was dissected lateral to the paraspinous muscles, and the ovaries were found. One ovary was pulled out through the incision by grasping the periovarian fat. The fallopian tube, uterine horn, and ovary were ligated and cut with scissors. The contralateral ovary was removed in an identical fashion, and the incision was closed and cleaned. For SHAM operations, ovaries were observed, pulled out through the incision by grasping the periovarian fat, and placed back through the incision. The incision was closed and cleaned. After surgery, mice were allowed to recover on a LFD or a HFD for 5 weeks.

Surgical catheterization

Surgical procedures involving catheterization in mice have been described by Ayala et al (28). Briefly, 5 weeks after OVX or SHAM operation and diet feeding, mice were anesthetized, and the carotid artery and jugular vein were catheterized. Free catheter ends were tunneled under the skin to the back of the neck, externalized, and sealed with steel plugs. These methods permit arterial sampling and are less stressful than cut-tail sampling (29). Mice were individually housed and allowed to recover for 5–7 days on their respective diets after surgery for a total of 6 weeks of diet feeding. All mice studied had returned to within 10% of their presurgical body weight before the study. Body fat composition was determined 1 day before experimentation using an mq10 NMR analyzer (Bruker Optics).

Hyperglycemic clamp studies

On the day of study, mice were fasted for 5 h. At $t = 0$ min, a variable rate of 50% dextrose was infused into the jugular line to increase and maintain blood glucose at 250–300 mg/dl (15 mmol/l) to provide matched blood glucose levels and promote hepatic glucose uptake. Insulin secretion was under endogenous control. Arterial blood glucose (5 μ l) was measured by glucometer at $t = -10, 0, 5, 10, 15,$ and 20 min and then every 10 min until $t = 150$ min. Arterial samples to measure plasma insulin and lipids were taken at $t = -10, 60,$ and 150 min. At 150 min, mice were euthanized, and tissues were collected and frozen in liquid nitrogen.

Whole cell extracts

Whole cell liver extracts were prepared using the T-Per tissue Extraction Reagent according to the manufacturer's protocol (Prod. 78510; Pierce,).

Western blots

Total protein (25 μ g), determined by BCA assay, was diluted into Nupage sample buffer and resolved in Nupage 4–12% Bis-Tris gels at 150V for 1 h. Samples were transferred onto a nitrocellulose membrane in MOPS running buffer supplemented with 20% methanol. Primary antibodies for ABCA1 and LDL

receptor (LDLR) were purchased from ABCAM (Cambridge, MA). Primary antibody for SR-BI was purchased from Santa Cruz Biotechnology. All primary antibodies were diluted 1:1000. We used 1:10,000 fluorescent secondary antibodies IRDye 800 anti-mouse, IRDye 680 anti-rabbit, and IRDye-800 anti-goat (LI-COR Biotechnology, Lincoln, NE). Images were acquired with the Odyssey infrared imaging system.

Serum insulin values

Serum insulin values were measured from 10 μ l of serum assayed in duplicate by ELISA according to the manufacturer's protocol (Cat# EZRMI-13K; Millipore).

HPLC and lipid assays

We used HPLC separation of serum lipoproteins to quantify the distribution of lipoproteins and define the composition of HDL. The aqueous buffers of HPLC avoid the high ionic strength of KBr ultracentrifugation, which is known to dissociate HDL-associated proteins. HPLC analysis was performed as described (30). Serum (100 μ l) from each animal was fractionated on a Superose-6 300 μ l column (GE Biosciences), and 300- μ l fractions were collected in a 96-well plate. Cholesterol content was assayed from the fractions using a kit from Raichem (cat# 85460). For area-under-the-curve analysis, VLDL fractions were defined as fractions 8–15, LDL as fractions 16–31, and HDL as fractions 32–54.

Serum TG and cholesterol assays

Serum (5 μ l) was diluted 1:10 and assayed for total TG and cholesterol levels using commercially available kits (prod. # 85460 and 84098; Raichem,).

Serum CETP activity assay

Serum (1 μ l) was assayed for CETP enzyme activity according to the manufacturer's protocol (# RB-CETP; Roar Biomedical).

Statistical analysis

Data were presented as means \pm SEM. Differences between groups ($n = 3$ – 9 animals per group) were determined by ANOVA followed by Tukey's post hoc tests or by two-tailed *t*-test as appropriate. Significance was flagged by $P < 0.05$.

HDL proteomics

We conducted protein identification from pooled HPLC fractions that corresponded to HDL from individual mice (Fractions 34–46 from Fig. 4). The samples were analyzed by multidimensional protein identification technology (MudPIT) and tandem mass spectrometry (31). Aliquots of HDL (50 μ g total protein) were dissolved in 20 μ l of TFE and 1 M TRIS at pH 8.0, and the cysteine residues were reduced with 0.5 M TCEP and alkylated with 1 M iodoacetamide. After dilution with buffer to 10% TFE, 2 μ g of trypsin was added and allowed to digest the proteins overnight at 37°C. The resulting tryptic peptides were analyzed via MudPIT analysis, essentially as described by MacCoss et al (32, 33). Briefly, peptides were loaded via a pressure cell (New Objective, Woburn, MA) onto a biphasic precolumn fritted using an Upchurch M-520 filter union. This 150- μ m fused silica capillary column was packed with 3 cm of 5- μ m C18 reverse-phase resin (Jupiter; Phenomenex) followed by 4 cm of strong cation-exchange resin (Luna SCX; Phenomenex). Once loaded, it was then placed in-line with a 100 μ m \times 20 cm C18 nanoflow reverse-phase column (3 μ m, 300 Å, Jupiter C18; Phenomenex, Torrance, CA). LC-MS/MS analysis was conducted on an LTQ linear ion trap mass spectrometer (Thermo Scientific, West Palm Beach, FL) equipped with an Eksigent NanoLC-AS1 Autosampler

V2.08, an Eksigent NanoLC-1D plus HPLC pump, and a nano-spray ion source. Multidimensional separations were accomplished using sequential 5 μ l pulses of ammonium acetate in 0.1% formic acid (100, 250, 500, and 1000 mM pulses). Each salt pulse was followed by a 115 min reversed phase gradient from 2% acetonitrile in 0.1% aqueous formic acid to 40% ACN in aqueous 0.1% formic acid. Tandem mass spectra were collected throughout the runs using a sequence of one precursor ion scan followed by acquisition of five product ion scans of the most abundant peptides using a data-dependent acquisition protocol.

Proteome bioinformatics

Having generated MudPIT data reflecting the response from HDL of individual mice, we used peer-reviewed tools for comparative proteomics. First, the data were transformed to mzML format by the ProteoWizard library (34). The tandem mass spectra in these files were matched to the proteins of RefSeq Mouse, build 37, version 2. The FASTA was augmented by the addition of 71 common contaminant sequences as well as CETP_MACFA, the macaque cholesteryl ester transfer protein. The reversed version of each of these proteins was added to the database for false discovery rate (FDR) estimation. Peptide identification took place via the MyriMatch database searching tool (35). IDPicker was used to conduct the process of protein assembly: filtering peptides to a confident set that achieves a specified FDR, organizing a set of LC-MS/MS experiments into a single experimental hierarchy, and applying parsimony to protein lists (36, 37). IDPicker was configured to require two distinct peptides and at least five spectra of each reported protein, with a 3% FDR at the level of peptide-spectrum matches. The complete ID picker report is available as a .zip file for download in the supplementary information, as is a link to download the raw LC-MS/MS data.

The resulting reports, differentiating between shared and distinct peptides for each protein group, give the number of spectra observed for each protein group across all data sets. These tables were used as the input for the QuasiTel tool, which applies a quasi-likelihood model to seek significant protein differences between pairs of cohorts (38). The software applies multiple testing correction to generate quasi *P* values for each difference. QuasiTel was configured to require one spectrum per biological replicate in at least one cohort for protein inclusion to reduce the number of statistical tests conducted. Venn diagrams were created with software created by J.C. Oliveros (<http://bioinfopg.cnb.csic.es/tools/venny/index.html>) using proteins that were identified as *mus musculus* and *macaca fascicularis* (these mice express simian CETP). A .zip file of the IDPicker report is available in the supplementary information. The RAW LC-MS/MS data are available for download from www.mc.vanderbilt.edu/msrc/bioinformatics/data.php.

RESULTS

High-fat feeding induces weight gain and hyperinsulinemia in ovariectomized mice without changes in CETP expression

To define the effects of surgical menopause and high-fat feeding on HDL composition, female CETP mice underwent surgical menopause by OVX and were fed a high-fat diet (HFD) for 6 weeks. After OVX, CETP mice were highly susceptible to diet-induced obesity with HFD-feeding, whereas no weight gain was observed in OVX mice following a low-fat diet (LFD). HFD-feeding did not induce weight gain in SHAM mice (Fig. 1A). As an index of peripheral insulin sensitivity, we measured fasting glucose and insulin

levels. There were no significant differences in fasting glucose values between groups (Fig. 1B). HFD feeding in the SHAM and OVX groups was associated with a trend toward elevated insulin values (174.7 ± 66.8 pmol/l and 342.1 ± 80.2 pmol/l, respectively) (Fig. 1C). There were no significant differences in CETP enzyme activity between groups (Fig. 1D) because these mice constitutively express the simian CETP gene. These results suggest that the presence of ovarian hormones protects against diet-induced obesity but does not prevent insulin resistance based on elevated fasting serum insulin levels. Additionally, increases in body weight after high-fat feeding observed in CETP mice after OVX recapitulate a predisposition to weight gain associated with menopause without changes in CETP activity in this model.

Absence of ovarian hormones worsens high-fat diet-induced glucose intolerance

Impaired glucose metabolism after menopause is associated with abnormalities in serum VLDL and HDL. To determine if OVX results in impaired glucose metabolism, we performed hyperglycemic clamp studies in which blood glucose was clamped at 250–300 mg/dl (Fig. 2A). This approach allows us to match blood glucose levels in mice with different body weights and different degrees of insulin sensitivity. Baseline glucose values were not different between groups, and blood glucose levels were clamped at a similar level of hyperglycemia for all groups (Fig. 2A). The amount of glucose infused required to maintain a similar level of hyperglycemia is an index of

glucose tolerance (i.e., glucose infusion rate [GIR]; Fig. 2B). High-fat feeding reduced the GIR required to maintain hyperglycemia in OVX-HFD-fed mice and in SHAM-HFD-fed mice compared with their LFD-fed controls (Fig. 2B, circles for OVX and triangles for SHAM; $P < 0.05$ for each). There was no difference in the GIR between OVX-LFD and SHAM-LFD mice. HFD-OVX mice had the lowest glucose infusion rate of any group, suggesting that the absence of ovarian hormones worsens the impact of HFD feeding on glucose tolerance (Fig. 2B).

During the clamp studies, we did not infuse insulin; thus, insulin secretion was under endogenous control. This approach defines insulin secretion in response to a defined blood glucose change and provides an index of β -cell function, a key mediator of glucose tolerance. HFD feeding led to an increase in serum insulin levels in response to hyperglycemia for SHAM and OVX mice compared with SHAM-LFD control mice (Fig. 2C), consistent with the elevated fasting insulin levels in these groups (Fig. 1C). Likewise, OVX-LFD displayed elevated clamp insulin levels compared with SHAM-LFD mice (Fig. 2C, light gray bars), demonstrating that HFD feeding, OVX, or both lead to hyperinsulinemia. The finding that OVX-LFD mice had hyperinsulinemia despite a similar GIR to SHAM-LFD mice suggests that OVX impairs insulin sensitivity. Thus, OVX appears to produce insulin resistance without weight gain, whereas HFD feeding after OVX accelerates weight gain and insulin resistance. The presence of ovarian hormones (the SHAM groups) protects against weight gain on HFD but does not prevent insulin resistance with HFD feeding.

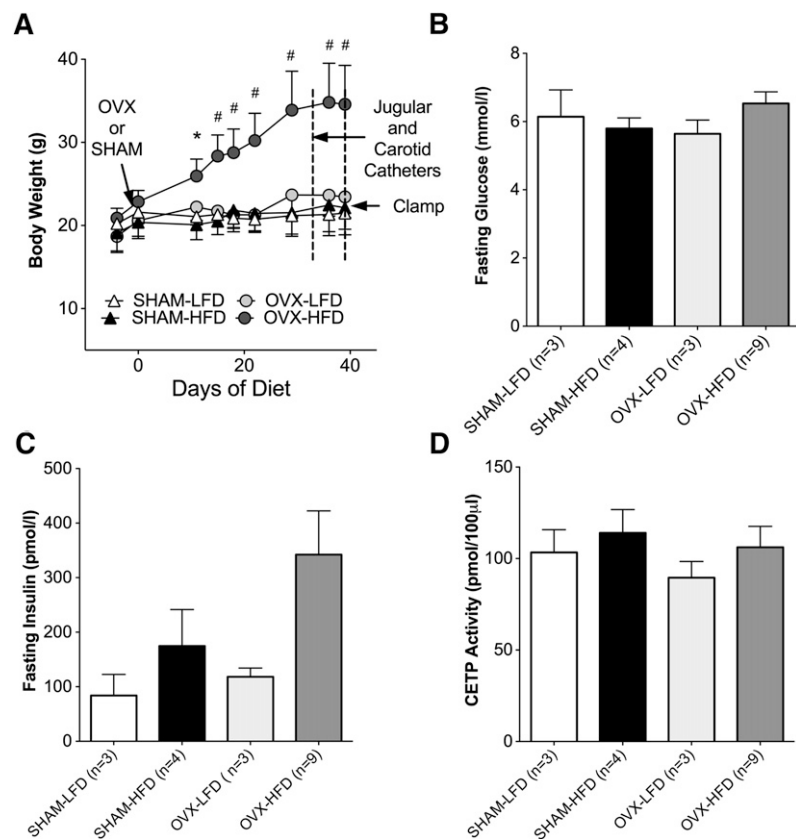


Fig. 1. HFD feeding after OVX promotes weight gain and hyperinsulinemia without changes in CETP expression. A: Body weight over 6 weeks of diet feeding. B: Fasting glucose values. C: Fasting insulin values. D: CETP activity. Results are expressed as means \pm SEM. Data were analyzed using ANOVA. * $P < 0.05$; # $P < 0.0001$.

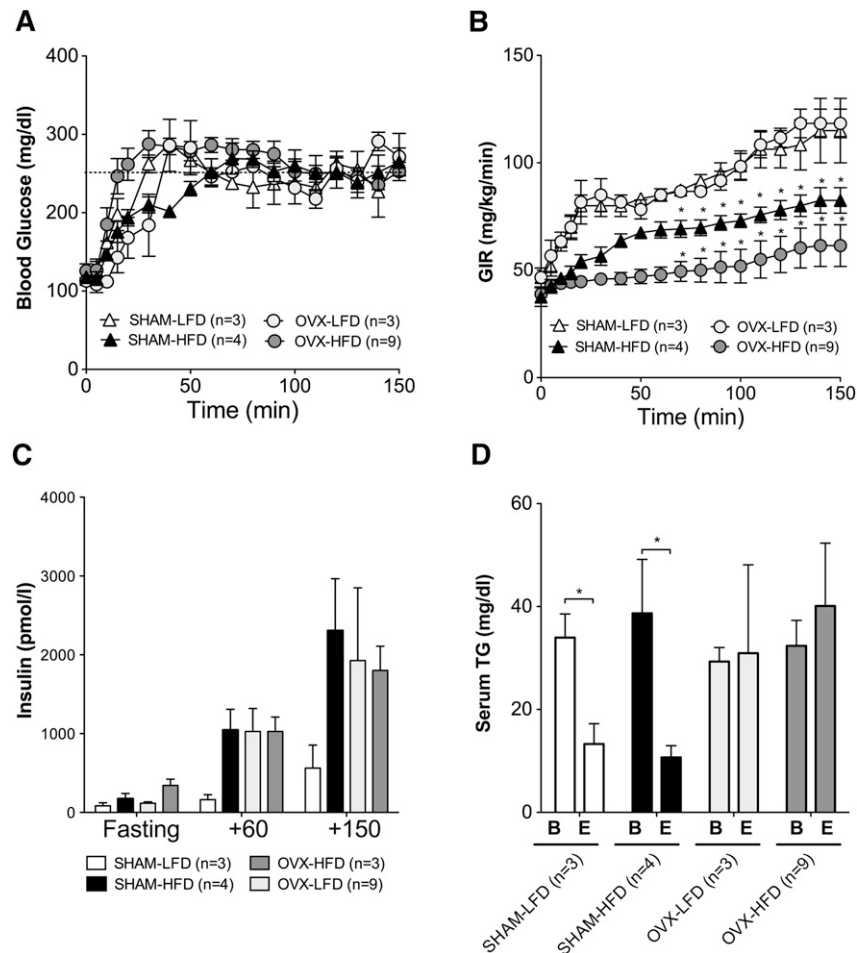


Fig. 2. Hyperglycemic clamp studies after OVX and high-fat diet feeding. Blood glucose values (A) and glucose infusion rates (GIR) (B) during the hyperglycemic clamp studies (the target blood glucose was 250–300 mg/dl). C: Insulin values during the clamp. D: Serum TG values before (baseline [B]) and after (endpoint [E]) the clamp. Results are expressed as means \pm SEM. Data were analyzed using ANOVA and comparisons made using Tukey's test. * $P < 0.05$.

Hyperinsulinemia does not lower serum triglyceride after ovariectomy

In vivo, insulin lowers serum TG levels by suppressing hepatic production of VLDL, blocking lipolysis and promoting TG clearance by adipose tissue (2, 39, 40). Failure of hyperglycemia and hyperinsulinemia to lower serum TG contributes to hypertriglyceridemia in obese women (18). To determine the ability of hyperinsulinemia to suppress serum TG levels, we measured serum TG at baseline [B] and at the endpoint [E] of the hyperglycemic clamp studies (Fig. 2D). Serum TG levels were not decreased in response to hyperinsulinemia after OVX in either the OVX-LFD or the OVX-HFD group (Fig. 2D). By contrast, despite HFD feeding, SHAM-operated mice had decreased TG levels after the clamp, suggesting that insulin appropriately suppresses serum TG when ovarian hormones are present (Fig. 2D). There were no significant differences in baseline TG levels between groups before hyperglycemia. Though these serum TG levels were in the normal range even during the clamp, these results suggest that loss of ovarian hormones impairs normal insulin regulation of serum TG levels in CETP mice.

Loss of ovarian hormones does not significantly alter HDL cholesterol content

Total serum cholesterol levels were similar in SHAM-LFD and SHAM-HFD mice (51 ± 11 and 60 ± 9 mg/dl). By contrast, OVX-HFD mice showed a 29% increase in cholesterol compared with SHAM-HFD mice (77 ± 13 and 60 ± 9 mg/dl). We separated lipoproteins by HPLC and determined the cholesterol content of VLDL, LDL, and HDL (Fig. 3A). In OVX-LFD mice, VLDL cholesterol was increased, but there were no significant differences in LDL/IDL or HDL cholesterol compared with SHAM-LFD mice (Fig. 3). In HFD-fed OVX mice, there was a nonsignificant increase in the cholesterol content of HDL fractions. SHAM-operated mice did not exhibit differences in VLDL, LDL, or HDL cholesterol with HFD feeding compared with LFD feeding (Fig. 3). Thus, OVX did not significantly change HDL cholesterol levels.

Expression of hepatic ABCA1, LDLR, and SR-B1 are reduced by the combined effect of HFD and OVX

To determine whether OVX and HFD feeding led to altered expression of hepatic proteins involved in lipoprotein

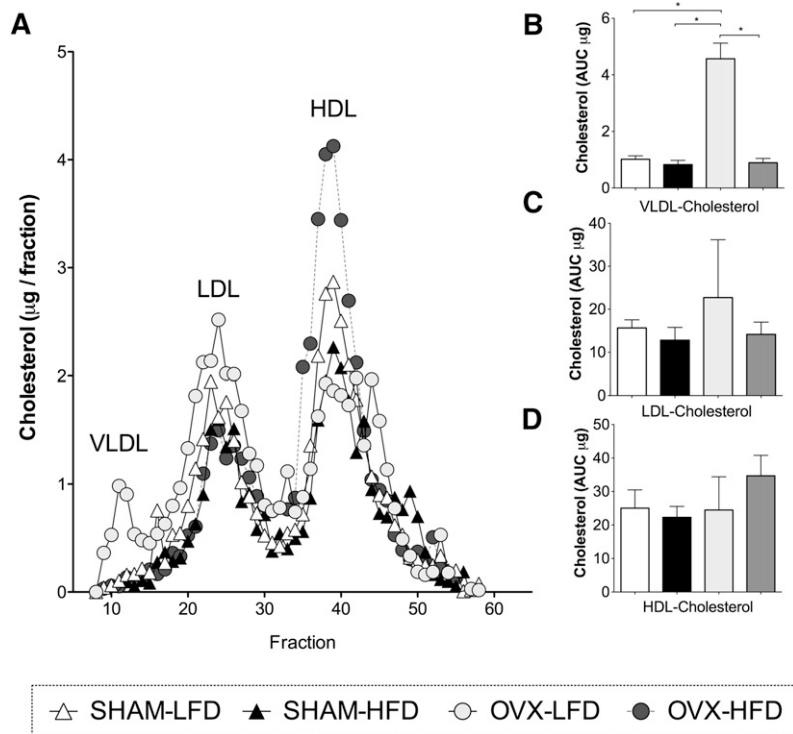


Fig. 3. Lipoprotein cholesterol distribution in CETP mice after hyperglycemia. **A:** Cholesterol content of lipoproteins separated by HPLC. Fractions corresponding to VLDL, LDL, and HDL are marked. **B:** Quantification of VLDL cholesterol based on the area under the curve (AUC). **C:** Quantification of LDL cholesterol based on the AUC. **D:** Quantification of HDL cholesterol based on the AUC. Results are expressed as means \pm SEM. Data were analyzed using ANOVA, and comparisons were made using Tukey's test. * $P < 0.05$.

clearance, we examined the expression of ATP-binding cassette subfamily A member 1 (ABCA1), LDLR and scavenger receptor class B1 (SR-B1). The expression of ABCA1 was significantly reduced after HFD-feeding in SHAM and OVX mice (Fig. 4A, B; $P < 0.0001$). There were no significant differences in ABCA1 expression after OVX alone compared with SHAM-LFD mice. The expression of LDLRs was significantly reduced in OVX-HFD compared with OVX-LFD (Fig. 4A, C; $P < 0.0001$). This diet effect on LDLR was only seen in OVX mice; there were no significant differences in the expression of LDLR in SHAM-HFD mice compared with SHAM-LFD fed mice. Similarly, the expression of SR-B1 was lower in OVX-HFD mice compared with the other groups (Fig. 4A, D; $P < 0.05$). The decreased expression of LDLR and SR-B1 are consistent with increased serum total cholesterol observed in mice fed OVX-HFD.

HFD feeding and loss of ovarian hormones independently affect HDL protein composition

To investigate how metabolic changes in glucose and TG metabolism associated with OVX and HFD feeding influence HDL composition, we performed a shotgun proteomic analysis of HDL. The total number of proteins identified in HDL fractions across all CETP groups was 408, counting only those that were evidenced by two distinct peptide sequences and five spectra among all experiments. The numbers of proteins found for SHAM-LFD, SHAM-HFD, OVX-LFD, OVX-HFD were 282, 320, 368, and 408, respectively (Fig. 5).

To determine the diversity of HDL protein composition, we generated a Venn diagram to illustrate shared and unique proteins for each group (Fig. 5). In OVX groups, we found 43 HDL proteins identified from HDL that were shared between OVX-LFD and OVX-HFD groups but not

present in HDL from either SHAM group. Thirty-seven proteins were unique to OVX-LFD, and 50 were unique to OVX-HFD. Thus, in the OVX groups, there were 130 unique proteins from HDL fractions that were not found in the SHAM groups. By comparison, only three proteins were unique to SHAM-LFD, and 13 were unique to SHAM-HFD. The proteins present in these categories are listed in Supplementary Table I. These results suggest that OVX induces a substantial change in the diversity of HDL protein composition compared with SHAM. The results further suggest that HFD feeding has a greater impact on the diversity of HDL protein composition in OVX mice.

We also defined the impact of OVX and HFD feeding on HDL composition by comparisons of shared HDL proteins between groups. There were 231 HDL proteins shared between all four groups (Fig. 5; see the gray area in center of the Venn diagram). Using peer-reviewed tools for comparative proteomics, four pair-wise comparisons were made between groups to generate a quasi- P value of statistical significance of HDL proteins between groups (34–38, 41, 42). Data for each comparison are organized as follows: 1) as a volcano plot of the log-change of all proteins compared between the groups, 2) a radar-plot illustrating log-changes in known HDL-associated proteins, and 3) as a supplementary table of known HDL proteins that includes spectral abundance and P value (Fig. 6; Supplementary Tables I–IV). The volcano and radar plots show the \log_2 of one group vs. another, which represents the relative abundance of HDL proteins. For instance, a \log_2 of 2 represents a 4-fold difference in spectral abundance of that protein between groups.

The major proteins in the HDL of all CETP mice included apoA-I, apoA-II, apoC-II, apoC-III, apoE, and apoM. There were no significant changes in the HDL-scaffold protein

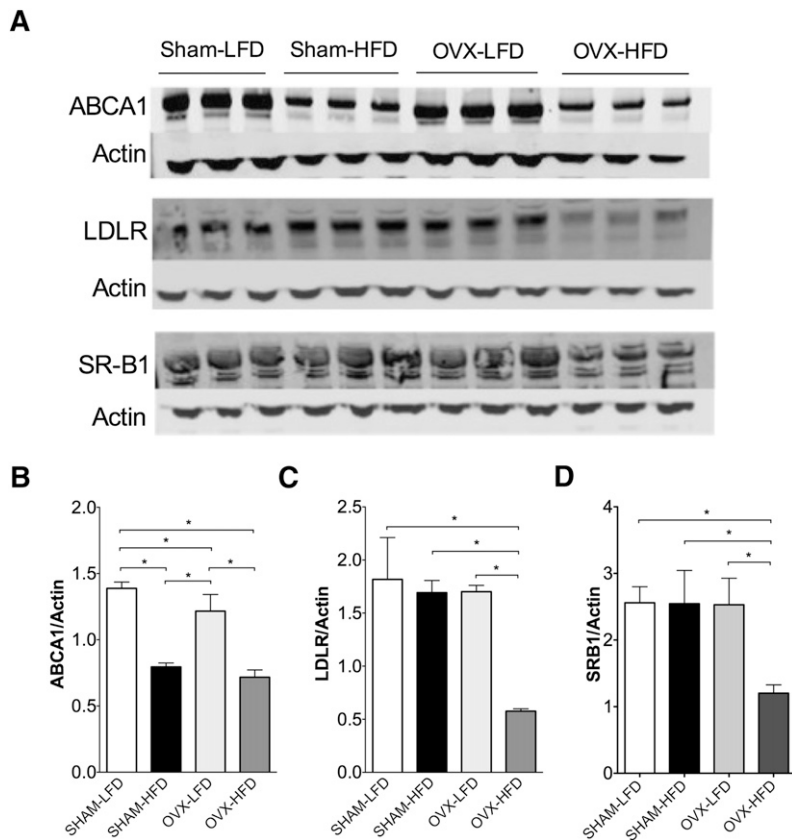


Fig. 4. Western blot analysis of ABCA1, LDL receptor, and SRB1 from whole-cell liver extracts. A: Western blot analysis of ABCA1, LDL receptor, and SRB1. B: Quantification of hepatic ABCA1 normalized to actin. C: Quantification of LDL receptor normalized to actin. D: Quantification of SR-B1 normalized to actin. Results are expressed as means SEM. Data were analyzed using ANOVA, and comparisons were made using Tukey's test. * $P < 0.05$.

apoA-I between groups (Supplementary Tables I–IV). The small amount of apoB indicates that minor contamination with nonHDL particles was present in these fractions. The normalized spectral counts for CETP in HDL were not different between groups, as predicted by our model where CETP expression and activity is constitutive.

We found relatively few changes in HDL proteins comparing SHAM-LFD vs. SHAM-HFD mice (Fig. 6A, E; Table 1; Supplementary Tables I and V). Only 15 of the 252 shared proteins were statistically significant. These included proteins involved in complement activation and innate immune system function (Supplementary Table V). Of proteins with known function in HDL, the notable statistically significant increases were in apoA-IV, apoC-II, and antithrombin III, although the magnitude of these increases was modest (Fig. 6A, E; Table 1). Supplementary Table I provides normalized spectral counts and P values for other proteins with known HDL function for SHAM-HFD compared with SHAM-LFD mice. The paucity of changes in HDL composition suggests that insulin resistance in SHAM mice (Fig. 2B and 2C) does not significantly alter HDL composition.

By contrast, HFD feeding in OVX mice resulted in more numerous changes in HDL composition because 68 of 312 HDL-associated proteins were significantly changed, compared with HDL from OVX-LFD mice (Fig. 6B). These represent proteins involved in coagulation, innate immune function, and lipid metabolism (Supplementary Table V). The radar plot with the ratio of abundance of known HDL proteins in OVX-HFD/OVX-LFD demonstrates that more proteins were upregulated by HFD feed-

ing after OVX (Fig. 6F) than HFD feeding after SHAM (Fig. 6E). As in SHAM mice, HFD feeding in OVX mice increased the apoA-IV, apoC-II, and antithrombin III content of HDL compared with OVX-LFD mice. We also saw increases in apoA-II, apoC-III, α -1 antitrypsin 1–5, and vitronectin (Fig. 6F; Table 1). Kininogen, a protein involved in the coagulation cascade, was significantly decreased. Supplementary Table II provides normalized spectral counts and P values for other proteins with known HDL function for OVX-HFD mice compared with OVX-LFD mice. These changes in shared HDL proteins mirror the more numerous unique HDL proteins in OVX mice shown

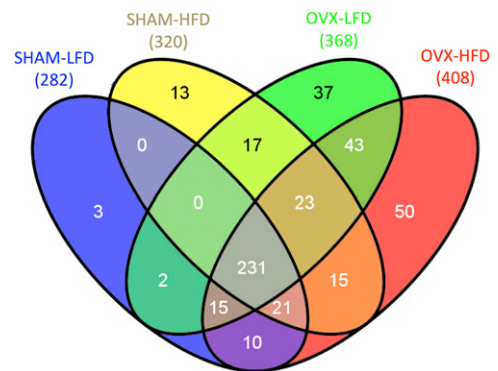


Fig. 5. Venn diagram showing shared and unique HDL-associated proteins for SHAM-LFD, SHAM-HFD, OVX-LFD, and OVX-HFD mice. Numbers in parentheses represent total number of protein identified for each group. Numbers in the shaded areas indicate the number of proteins for each group(s).

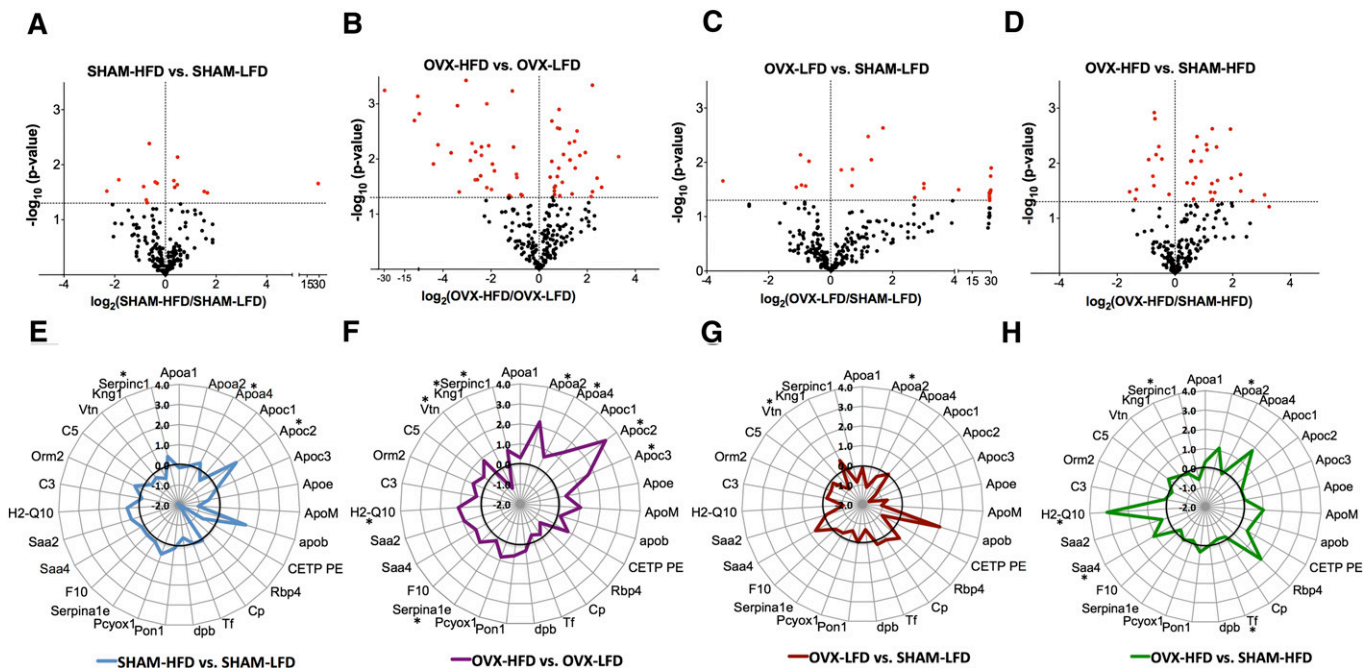


Fig. 6. HFD feeding and OVX differentially alter HDL-associated proteins. A–D: Volcano plot of protein abundance vs. *P* value for the difference, where the horizontal axis is the \log_2 (rate of group 2/rate of group 1), and vertical axis is $-\log_{10}$ (*P* value). E–H: Radar plot of protein abundance (\log_2 (rate of group 2/rate of group 1)). The radar plots are organized by gene. *Significantly altered proteins in radar plots; quasi *P* < 0.05.

in the Venn diagram in Fig. 5. These data suggest that HFD feeding has a greater impact on HDL composition in the absence of ovarian hormones.

The comparisons above define the impact of HFD feeding depending on whether the mice received OVX or SHAM operation. To define the impact of OVX on HDL composition compared with SHAM, we compared HDL from OVX mice with SHAM mice on the same diet. In LFD-fed mice, loss of ovarian hormones by OVX was associated with 29 changes of

the 248 proteins shared between SHAM-LFD and OVX-LFD (Fig. 6C). There were relatively few changes in proteins with known HDL function (Fig. 6G, few proteins deviate from the bold line; Supplementary Table III). To define the impact of OVX on HDL composition in mice maintained on a HFD, we compared HDL composition between OVX-HFD and SHAM-HFD mice. In HFD-fed mice, we found that OVX was associated with 37 protein changes of the 290 HDL-associated proteins shared between mice (Fig. 6D). We found increased

TABLE 1. Significantly altered HDL proteins grouped by each of the four pair-wise comparisons made

Gene Name	Change in Protein Abundance	Quasi <i>P</i> value	Protein Name/Function	Protein Function
Effect of HFD feeding in SHAM mice				
Apoa4	Increased	0.01946	Apolipoprotein A-IV	Lipid transport: activates LCAT, role in satiety
Apoc2	Increased	0.03054	Apolipoprotein C-II	Lipid metabolism: activates lipoprotein lipase
Serpinc1	Increased	0.00727	Antithrombin III	Coagulation: inhibits the coagulation cascade
Effect of HFD feeding in OVX mice				
Apoa2	Increased	0.00046	Apolipoprotein A-II	Lipid transport: stabilizes HDL particles
Apoa4	Increased	0.03284	Apolipoprotein A-IV	Lipid transport: activates LCAT, role in satiety
Apoc2	Increased	0.00907	Apolipoprotein C-II	TG metabolism: activates lipoprotein lipase
Apoc3	Increased	0.00860	Apolipoprotein C-III	TG and Lipid metabolism: inhibits LPL and HL
Serpina1e	Increased	0.01466	Alpha-1-antitrypsin 1-5	Protease inhibition: regulates proteolysis
Vtn	Increased	0.00126	Vitronectin	Cell adhesion and migration: binds to (PAI-1)
Kng1	Decreased	0.00058	Kininogen	Coagulation
Serpinc1	Increased	0.02076	Antithrombin III	Coagulation: inhibits the coagulation cascade
Effect of OVX in LFD fed mice				
Apoa2	Decreased	0.02883	Apolipoprotein A-II	Lipid transport: stabilizes HDL particles
Vtn	Decreased	0.00727	Vitronectin	Cell adhesion and migration: binds to (PAI-1)
Effect of OVX in HFD fed mice				
Apoa2	Increased	0.00575	Apolipoprotein A-II	Lipid transport: stabilizes HDL particles
Tf	Decreased	0.03676	Serotransferrin	Iron metabolism
Saa4	Increased	0.00459	Serum amyloid A-4 protein	Acute phase response: mediates HDL-VLDL interactions
H2-Q10	Increased	0.03760	H-2 class I HC antigen	Antigen processing and presentation
Serpinc1	Decreased	0.00499	Antithrombin III	Coagulation: inhibits the coagulation cascade

ApoA-IV, SAA4, and H2-Q10 (Fig. 6H; Table 1). Overall, these results suggest that OVX differentially affects HDL composition depending on the metabolic context, such as HFD feeding.

DISCUSSION

Risk factors of cardiovascular disease associated with obesity include insulin resistance, impaired glucose tolerance, elevated serum TG, low HDL, and loss of HDL's protective cardiovascular effects. From human studies, HDL proteomics have revealed numerous HDL-associated proteins and have suggested functional properties of HDL related to lipid transfer, inflammation, coagulation, and immunity (8–12). These studies have shown that some HDL proteins are altered in patients with CHD, suggesting that HDL can lose its ability to protect from CHD and may lead to an increased risk of CHD. Despite these strong associations, mechanisms that link metabolic changes with altered HDL composition have been more limited because the most common model of metabolic disease—the mouse—lacks CETP expression. In these studies, we have defined the HDL proteome of female CETP-expressing mice and characterized the impact of acute metabolic changes induced by HFD feeding and loss of ovarian hormones. We found that HDL composition in CETP mice is dynamically altered by changes in metabolism associated with obesity and that the impact of HFD feeding on HDL composition is dependent on metabolic context. CETP-expressing mice were susceptible to HFD-induced changes in HDL composition after OVX but were relatively resistant to diet-induced changes in HDL composition after a sham operation.

With the experimental approach of combining measurements of *in vivo* metabolism with HDL proteomics in CETP-expressing mice, we were able to establish metabolic relationships that contribute to changes in HDL composition. We found a differential impact of HFD feeding on several aspects of metabolism that contribute to cardiovascular risk, depending on ovarian hormone status. CETP mice gained weight on HFD feeding after OVX, whereas SHAM-operated CETP mice did not. The absence of weight gain with HFD feeding in the SHAM group may be attributable to metabolic differences caused by CETP expression. In similar experiments with nonCETP-expressing C57/B6J mice, there was a 20% weight gain with this duration of feeding (Martinez and Stafford, unpublished observation).

Despite being protected from weight gain, SHAM-operated CETP mice were not protected from impaired glucose tolerance and insulin resistance with HFD feeding. With our hyperglycemic clamp approach, we were able to look at two aspects of glucose metabolism that correlate with metabolic disease, glucose tolerance, and insulin secretory capacity. We found that HFD feeding in SHAM mice led to impaired glucose tolerance, as mice in this group required less glucose to maintain hyperglycemia than SHAM mice fed LFD. The degree of impaired glucose tolerance with HFD feeding was worsened with OVX

compared with SHAM mice. Because insulin secretion was under endogenous control during these studies, we were able to use insulin secretory capacity as a second measure of glucose metabolism. Compared with SHAM mice fed LFD, we found all of the other groups were insulin resistant, as indicated by hyperinsulinemia in response to a matched change in blood glucose. These findings demonstrate that ovarian hormones only partially prevent insulin resistance with HFD feeding. By contrast, the presence of ovarian hormones had a large protective effect against diet-induced weight gain.

The presence of ovarian hormones also maintained insulin's effect to suppress serum TG, even with HFD feeding, as the SHAM-LFD and SHAM-HFD groups both had normal suppression of serum TG after hyperglycemia and hyperinsulinemia. Hyperinsulinemia did not lower serum TG after OVX, even for lean LFD-fed mice. This biology is consistent with the increased VLDL-TG secretion rate associated with loss of ovarian hormones in humans (19). Thus, despite an absence of weight gain, CETP mice after OVX do not suppress serum TG levels in response to insulin, which might affect HDL because of lipid transfer mediated by CETP.


A major objective of these studies was to identify how defined changes in metabolism associated with obesity affect HDL composition. We found substantial overlap in HDL-associated proteins in CETP mice compared with published proteomes from human HDL (12). Human studies have established the importance of HDL composition as an index of HDL function. However, these studies are somewhat limited in establishing cause and effect of metabolic changes and HDL composition because they often represent samples from a single chronological point and cannot take into account inherent heterogeneity in body weight, lipid metabolism, and genetics. In our studies we have used inbred CETP mice, which are genetically homogeneous and were matched for body composition at baseline. We also chose to use mice constitutively expressing the simian CETP gene to avoid confounding in CETP expression associated with obesity, diet, and changes in ovarian hormones status. In our studies, we defined changes in HDL composition due to changes in diet, changes in response to OVX, and the interaction of both. We found that impairments in TG metabolism related most significantly with ovarian hormone status. Impairments in insulin sensitivity occurred with HFD-feeding in SHAM mice but were exaggerated by OVX. Regarding the protein composition of HDL, we found that most changes were due to HFD-feeding in OVX mice, compared with HFD-feeding in SHAM mice.

We used two strategies to compare HDL composition from the four groups. First, we looked at the diversity of HDL proteins using a Venn diagram. We found a large number of proteins unique to the HDL groups but relatively few proteins unique to the SHAM groups. We found 130 proteins unique to OVX-LFD, to OVX-HFD, or shared between both, but these proteins were not present in HDL from SHAM mice. The significance of many of these proteins regarding HDL function remains to be determined,

but we observed a wide array of proteins related to immune function, coagulation, and lipid metabolism. This is in contrast to the SHAM groups, for which we found only 16 proteins unique to SHAM-LFD, to SHAM-HFD, or shared between both. The abundance of proteins identified by our approach may reflect the HPLC separation process used, which is more likely to preserve loosely associated HDL proteins compared with high-salt buffers used with ultracentrifugation (8). The presence of proteins involved in glucose metabolism uniquely in the OVX groups may substantiate the relationship of impaired glucose metabolism with HDL protein changes after OVX. Thus, the Venn diagrams illustrate that OVX in CETP mice generates a dynamic change to HDL composition. Furthermore, the Venn diagram suggests that HFD feeding generates more protein changes in HDL when ovarian hormones are absent.

When we restricted our analysis to shared proteins between groups, we saw a larger impact of HFD feeding after OVX than in SHAM mice. We found that HFD feeding significantly altered 21% of the HDL proteins after OVX (68 proteins changed of 312 proteins shared), compared with less than 6% of HDL proteins altered with HFD feeding after SHAM (15 of 252 proteins were different). The low number of mice is a limitation to interpreting the percent of proteins that were significantly different between groups. Further evidence supporting a more robust impact of HFD feeding on HDL composition after OVX is that the fold-change in protein levels was greater after OVX than after HFD feeding for SHAM mice (Fig. 6E–H). From the OVX-HFD group, we found increases in ApoA-II and ApoC-III that were not noted with HFD feeding in SHAM mice. These changes could result from, or contribute to, the absence of insulin suppression of serum TG seen in OVX mice (Fig. 2D). We cannot exclude that differences in insulin action contributed to differences in HDL composition between HFD-fed SHAM and OVX mice; however, both groups were similarly hyperinsulinemic during the hyperglycemic clamp study, making this less likely. These findings suggest that the presence of ovarian hormones helps protect from atherogenic changes in HDL composition in the setting of HFD feeding. These studies help define the impact of HFD feeding, loss of ovarian hormones, and the interaction of both regarding HDL composition.

Many studies of menopause and cardiovascular risk factors in humans have been cross-sectional, comparing women before and after menopause. As a result, these studies did not characterize the relative impact of acute loss of ovarian hormones toward cardiovascular risk at menopause, as opposed to normal aging and weight gain (43–45). To address this, the Study of Women's Health Across the Nation (SWAN) followed women from premenopause to postmenopause and found that, although aging influences obesity and waist circumference, menopausal status independently influenced HDL levels (46). Similarly, sex and obesity differentially affect VLDL secretion in humans (47). The results presented here define the HDL proteome of female CETP mice

and further relate changes in HDL composition to a well defined physiologic assessment of body weight, body composition, and clamp-defined glucose and TG metabolism. These data demonstrate that there are large changes in protein composition in HDL that are not revealed by measurement of the cholesterol content of HDL. Although there are changes in lipoprotein levels and composition that are not fully recapitulated in humans, these results suggest that CETP-expressing mice can be used as a mouse model to provide insight into how HDL composition changes in response to metabolic interventions. 

The authors acknowledge excellent assistance by the Vanderbilt Mouse Metabolic Phenotyping Center, the Vanderbilt Proteomics and Mass Spectrometry Core, and the Vanderbilt Hormone Assay Core.

REFERENCES

- Lamarque, B., K. D. Uffelman, A. Carpentier, J. S. Cohn, G. Steiner, P. H. Barrett, and G. F. Lewis. 1999. Triglyceride enrichment of HDL enhances in vivo metabolic clearance of HDL apo A-I in healthy men. *J. Clin. Invest.* **103**: 1191–1199.
- Lewis, G. F., K. D. Uffelman, L. W. Szeto, B. Weller, and G. Steiner. 1995. Interaction between free fatty acids and insulin in the acute control of very low density lipoprotein production in humans. *J. Clin. Invest.* **95**: 158–166.
- Horowitz, B. S., I. J. Goldberg, J. Merab, T. M. Vanni, R. Ramakrishnan, and H. N. Ginsberg. 1993. Increased plasma and renal clearance of an exchangeable pool of apolipoprotein A-I in subjects with low levels of high density lipoprotein cholesterol. *J. Clin. Invest.* **91**: 1743–1752.
- Van Lenten, B. J., S. Y. Hama, F. C. de Beer, D. M. Stafforini, T. M. McIntyre, S. M. Prescott, B. N. La Du, A. M. Fogelman, and M. Navab. 1995. Anti-inflammatory HDL becomes pro-inflammatory during the acute phase response: loss of protective effect of HDL against LDL oxidation in aortic wall cell cocultures. *J. Clin. Invest.* **96**: 2758–2767.
- Eckel, R. H., W. W. Barouch, and A. G. Ershow. 2002. Report of the National Heart, Lung, and Blood Institute-National Institute of Diabetes and Digestive and Kidney Diseases Working Group on the pathophysiology of obesity-associated cardiovascular disease. *Circulation.* **105**: 2923–2928.
- Goldberg, I. J., R. H. Eckel, and R. McPherson. 2011. Triglycerides and heart disease: still a hypothesis? *Arterioscler. Thromb. Vasc. Biol.* **31**: 1716–1725.
- Brinton, E. A., S. Eisenberg, and J. L. Breslow. 1989. Elevated high density lipoprotein cholesterol levels correlate with decreased apolipoprotein A-I and A-II fractional catabolic rate in women. *J. Clin. Invest.* **84**: 262–269.
- Collins, L. A., and M. Olivier. 2010. Quantitative comparison of lipoprotein fractions derived from human plasma and serum by liquid chromatography-tandem mass spectrometry. *Proteome Sci.* **8**: 42.
- Julve, J., J. C. Escola-Gil, N. Rotllan, C. Fievet, E. Vallez, C. de la Torre, V. Ribas, J. H. Sloan, and F. Blanco-Vaca. 2010. Human apolipoprotein A-II determines plasma triglycerides by regulating lipoprotein lipase activity and high-density lipoprotein proteome. *Arterioscler. Thromb. Vasc. Biol.* **30**: 232–238.
- Davidsson, P., J. Hulthe, B. Fagerberg, and G. Camejo. 2010. Proteomics of apolipoproteins and associated proteins from plasma high-density lipoproteins. *Arterioscler. Thromb. Vasc. Biol.* **30**: 156–163.
- Stahlman, M., P. Davidsson, I. Kanmert, B. Rosengren, J. Boren, B. Fagerberg, and G. Camejo. 2008. Proteomics and lipids of lipoproteins isolated at low salt concentrations in D₂O/sucrose or in KBr. *J. Lipid Res.* **49**: 481–490.
- Vaisar, T., S. Pennathur, P. S. Green, S. A. Gharib, A. N. Hoofnagle, M. C. Cheung, J. Byun, S. Vuletic, S. Kassim, P. Singh, et al. 2007. Shotgun proteomics implicates protease inhibition and complement

- activation in the antiinflammatory properties of HDL. *J. Clin. Invest.* **117**: 746–756.
13. Navab, M., S. Y. Hama, G. P. Hough, G. Subbanagounder, S. T. Reddy, and A. M. Fogelman. 2001. A cell-free assay for detecting HDL that is dysfunctional in preventing the formation of or inactivating oxidized phospholipids. *J. Lipid Res.* **42**: 1308–1317.
 14. Lewis, G. F., and D. J. Rader. 2005. New insights into the regulation of HDL metabolism and reverse cholesterol transport. *Circ. Res.* **96**: 1221–1232.
 15. Fazio, S., and M. F. Linton. 2010. High-density lipoprotein therapeutics and cardiovascular prevention. *J. Clin. Lipidol.* **4**: 411–419.
 16. Khera, A. V., M. Cuchel, M. de la Llera-Moya, A. Rodrigues, M. F. Burke, K. Jafri, B. C. French, J. A. Phillips, M. L. Mucksavage, R. L. Wilensky, et al. 2011. Cholesterol efflux capacity, high-density lipoprotein function, and atherosclerosis. *N. Engl. J. Med.* **364**: 127–135.
 17. Feingold, K. R., and C. Grunfeld. 2010. The acute phase response inhibits reverse cholesterol transport. *J. Lipid Res.* **51**: 682–684.
 18. Mittendorfer, B., B. W. Patterson, S. Klein, and L. S. Sidossis. 2003. VLDL-triglyceride kinetics during hyperglycemia-hyperinsulinemia: effects of sex and obesity. *Am. J. Physiol. Endocrinol. Metab.* **284**: E708–E715.
 19. Magkos, F., E. Fabbrini, B. S. Mohammed, B. W. Patterson, S. Klein, and B. Mittendorfer. 2010. Estrogen deficiency after menopause does not result in male very-low-density lipoprotein metabolism phenotype. *J. Clin. Endocrinol. Metab.* **95**: 3377–3384.
 20. Horton, T. J., E. C. Gayles, P. A. Prach, T. A. Koppenhafer, and M. J. Pagliassotti. 1997. Female rats do not develop sucrose-induced insulin resistance. *Am. J. Physiol.* **272**: R1571–R1576.
 21. Masucci-Magoulas, L., A. Plump, X. C. Jiang, A. Walsh, J. L. Breslow, and A. R. Tall. 1996. Profound induction of hepatic cholesteryl ester transfer protein transgene expression in apolipoprotein E and low density lipoprotein receptor gene knockout mice: a novel mechanism signals changes in plasma cholesterol levels. *J. Clin. Invest.* **97**: 154–161.
 22. Marotti, K. R., C. K. Castle, T. P. Boyle, A. H. Lin, R. W. Murray, and G. W. Melchior. 1993. Severe atherosclerosis in transgenic mice expressing simian cholesteryl ester transfer protein. *Nature.* **364**: 73–75.
 23. Jiang, X. C., L. B. Agellon, A. Walsh, J. L. Breslow, and A. Tall. 1992. Dietary cholesterol increases transcription of the human cholesteryl ester transfer protein gene in transgenic mice: dependence on natural flanking sequences. *J. Clin. Invest.* **90**: 1290–1295.
 24. Berti, J. A., A. C. Casquero, P. R. Patricio, E. J. B. Bighetti, E. M. Carneiro, A. C. Boschero, and H. C. F. Oliveira. 2003. Cholesteryl ester transfer protein expression is down-regulated in hyperinsulinemic transgenic mice. *J. Lipid Res.* **44**: 1870–1876.
 25. Arai, T., S. Yamashita, K. Hirano, N. Sakai, K. Kotani, S. Fujioka, S. Nozaki, Y. Keno, M. Yamane, E. Shinohara, et al. 1994. Increased plasma cholesteryl ester transfer protein in obese subjects: a possible mechanism for the reduction of serum HDL cholesterol levels in obesity. *Arterioscler. Thromb.* **14**: 1129–1136.
 26. Magkos, F., B. S. Mohammed, and B. Mittendorfer. 2009. Plasma lipid transfer enzymes in non-diabetic lean and obese men and women. *Lipids.* **44**: 459–464.
 27. Marotti, K. R., C. K. Castle, R. W. Murray, E. F. Rehberg, H. G. Polites, and G. W. Melchior. 1992. The role of cholesteryl ester transfer protein in primate apolipoprotein A-I metabolism: insights from studies with transgenic mice. *Arterioscler. Thromb.* **12**: 736–744.
 28. Ayala, J. E., V. T. Samuel, G. J. Morton, S. Obici, C. M. Croniger, G. I. Shulman, D. H. Wasserman, and O. P. McGuinness. 2010. Standard operating procedures for describing and performing metabolic tests of glucose homeostasis in mice. *Dis. Model Mech.* **3**: 525–534.
 29. Ayala, J. E., D. P. Bracy, O. McGuinness, and D. H. Wasserman. 2006. Considerations in the design of hyperinsulinemic-euglycemic clamps in the conscious mouse. *Diabetes.* **55**: 390–397.
 30. Hasty, A. H., H. Shimano, J. Osuga, I. Namatame, A. Takahashi, N. Yahagi, S. Perrey, Y. Iizuka, Y. Tamura, M. Amemiya-Kudo, et al. 2001. Severe hypercholesterolemia, hypertriglyceridemia, and atherosclerosis in mice lacking both leptin and the low density lipoprotein receptor. *J. Biol. Chem.* **276**: 37402–37408.
 31. Washburn, M. P., D. Wolters, and J. R. Yates 3rd. 2001. Large-scale analysis of the yeast proteome by multidimensional protein identification technology. *Nat. Biotechnol.* **19**: 242–247.
 32. MacCoss, M. J., W. H. McDonald, A. Saraf, R. Sadygov, J. M. Clark, J. J. Tasto, K. L. Gould, D. Wolters, M. Washburn, A. Weiss, et al. 2002. Shotgun identification of protein modifications from protein complexes and lens tissue. *Proc. Natl. Acad. Sci. USA.* **99**: 7900–7905.
 33. Link, A. J., J. Eng, D. M. Schieltz, E. Carmack, G. J. Mize, D. R. Morris, B. M. Garvik, and J. R. Yates 3rd. 1999. Direct analysis of protein complexes using mass spectrometry. *Nat. Biotechnol.* **17**: 676–682.
 34. Kessner, D., M. Chambers, R. Burke, D. Agus, and P. Mallick. 2008. ProteoWizard: open source software for rapid proteomics tools development. *Bioinformatics.* **24**: 2534–2536.
 35. Tabb, D. L., C. G. Fernando, and M. C. Chambers. 2007. MyriMatch: highly accurate tandem mass spectral peptide identification by multivariate hypergeometric analysis. *J. Proteome Res.* **6**: 654–661.
 36. Zhang, B., M. C. Chambers, and D. L. Tabb. 2007. Proteomic parsimony through bipartite graph analysis improves accuracy and transparency. *J. Proteome Res.* **6**: 3549–3557.
 37. Ma, Z. Q., S. Dasari, M. C. Chambers, M. D. Litton, S. M. Sobecki, L. J. Zimmerman, P. J. Halvey, B. Schilling, P. M. Drake, B. W. Gibson, et al. 2009. IDPicker 2.0: improved protein assembly with high discrimination peptide identification filtering. *J. Proteome Res.* **8**: 3872–3881.
 38. Li, M., W. Gray, H. Zhang, C. H. Chung, D. Billheimer, W. G. Yarbrough, D. C. Liebler, Y. Shyr, and R. J. Slebos. 2010. Comparative shotgun proteomics using spectral count data and quasi-likelihood modeling. *J. Proteome Res.* **9**: 4295–4305.
 39. Wu, K., D. Cappel, M. Martinez, and J. M. Stafford. 2010. Impaired inactivation of FoxO1 contributes to glucose-mediated increases in serum very low-density lipoprotein. *Endocrinology.* **151**: 3566–3576.
 40. Sadur, C. N., and R. H. Eckel. 1982. Insulin stimulation of adipose tissue lipoprotein lipase: use of the euglycemic clamp technique. *J. Clin. Invest.* **69**: 1119–1125.
 41. Dasari, S., M. C. Chambers, R. J. Slebos, L. J. Zimmerman, A. J. Ham, and D. L. Tabb. 2010. TagRecon: high-throughput mutation identification through sequence tagging. *J. Proteome Res.* **9**: 1716–1726.
 42. Dasari, S., M. C. Chambers, S. G. Codreanu, D. C. Liebler, B. C. Collins, S. R. Pennington, W. M. Gallagher, and D. L. Tabb. 2011. Sequence tagging reveals unexpected modifications in toxicoproteomics. *Chem. Res. Toxicol.* **24**: 204–216.
 43. Matthews, K. A., E. Meilahn, L. H. Kuller, S. F. Kelsey, A. W. Caggiula, and R. R. Wing. 1989. Menopause and risk factors for coronary heart disease. *N. Engl. J. Med.* **321**: 641–646.
 44. Mozaffarian, D., E. B. Rimm, and D. M. Herrington. 2004. Dietary fats, carbohydrate, and progression of coronary atherosclerosis in postmenopausal women. *Am. J. Clin. Nutr.* **80**: 1175–1184.
 45. Rossouw, J. E., R. L. Prentice, J. E. Manson, L. Wu, D. Barad, V. M. Barnabei, M. Ko, A. Z. LaCroix, K. L. Margolis, and M. L. Stefanick. 2007. Postmenopausal hormone therapy and risk of cardiovascular disease by age and years since menopause. *JAMA.* **297**: 1465–1477.
 46. Woodard, G. A., M. M. Brooks, E. Barinas-Mitchell, R. H. Mackey, K. A. Matthews, and K. Sutton-Tyrrell. 2011. Lipids, menopause, and early atherosclerosis in Study of Women's Health Across the Nation Heart women. *Menopause.* **18**: 376–384.
 47. Mittendorfer, B., B. W. Patterson, and S. Klein. 2003. Effect of sex and obesity on basal VLDL-triacylglycerol kinetics. *Am. J. Clin. Nutr.* **77**: 573–579.